Journal of Photochemistry and Photobiology A: Chemistry 346 (2017) 60–69

Contents lists available at ScienceDirect

Journal of Photochemistry and Photobiology A: Chemistry

journal homepage: www.elsevier.com/locate/jphotochem

Photocatalytic degradation of Rhodamine B dye by cotton textile coated with SiO_2-TiO_2 and SiO_2-TiO_2-HY composites

Salmon Landi Jr.[a,b,*], Joaquim Carneiro[a], Stanislav Ferdov[a], António M. Fonseca[c,d], Isabel C. Neves[c,d], Marta Ferreira[c], Pier Parpot[c,d], Olivia S.G.P. Soares[e], Manuel F.R. Pereira[e]

[a] Department of Physics, University of Minho, Azurém Campus, 4800-058 Guimarães, Portugal
[b] Instituto Federal Goiano, 75901-970, Rio Verde, Goiás, Brazil
[c] Center of Chemistry, Chemistry Department, University of Minho, Gualtar Campus, 4710-057 Braga, Portugal
[d] CEB—Centre of Biological Engineering, University of Minho, 4710-057 Braga, Portugal
[e] Laboratory of Catalysis and Materials—Associate Laboratory LSRE/LCM, Faculty of Engineering, University of Porto, 4200-465 Porto, Portugal

ARTICLE INFO

Article history:
Received 25 March 2017
Received in revised form 23 May 2017
Accepted 29 May 2017
Available online 2 June 2017

Keywords:
Photocatalysis
Textile functionalization
TiO_2-SiO_2
HY zeolite
Composites
Rhodamine B

ABSTRACT

This work is devoted to study the photocatalytic ability of cotton textiles functionalized with SiO_2-TiO_2 and SiO_2-TiO_2-HY composites to degrade a dye molecule. Coatings were prepared by sol-gel method and calcined at different temperatures in a range of 400–750 °C. FTIR confirmed the existence of Si—O—Ti bounds and the band located in the region between 570 and 600 cm^{-1} was used to calculate the framework Si/Al ratio of HY in the SiO_2-TiO_2-HY composites. XRD confirmed the presence of nanosized TiO_2 (anatase phase) in all calcined composites. Nitrogen adsorption isotherms showed a decrease in surface area and pore volume for higher calcination temperature. A simple mechanical process was used to impregnate the different composites on the cotton substrates. The photocatalytic activity of cotton textiles functionalized with SiO_2-TiO_2 and SiO_2-TiO_2-HY composites was tested via the degradation of Rhodamine B (RhB) dye under similar solar irradiation. The best catalytic performance was achieved with the SiO_2-TiO_2 and SiO_2-TiO_2-HY composites subjected to a calcination treatment at 400 °C, whereas SiO_2-TiO_2 presented a decolourization and mineralization around 94% and 89%, respectively, after 2 h of irradiation. Furthermore, the products of RhB degradation were analysed and identified by using HPLC-ESI–MS and ion chromatography techniques and a photocatalytic mechanism was proposed.

1. Introduction

The textile industry and their wastewaters contaminated with dyes cause a serious pollution problem around the world. According to O'Neill et al. [1], about 2–50% of textile dyes are released into the environment since some of the dye molecules do not bind to the fabrics during the dyeing processes. Discharging textile dyes into the water courses is unwanted, not only due to characteristics related to its colour, but also because many of these dyes and their corresponding degradation products are very toxic to living beings and surrounding ecosystems [2]. In this sense, it is important to develop processes in order to treat the wastewaters to ensure a sustainable environment. There are several wastewater treatments, such as biological, physical and chemical, for cleaning the water in order to achieve the desired level of water quality. Recently, advanced oxidation processes (AOPs) have been shown to be promising solutions for the removal of organic contaminants from wastewaters [3]. Among them, special attention is given to the use of photocatalytic systems through irradiation of titanium dioxide (TiO_2) nanoparticles [4]. Heterogeneous photocatalysis based in semiconductors is an important option because semiconductors can act as catalysts allowing easily mineralization of many organic compounds without additives [5]. Several catalysts such as TiO_2, ZnO, WO_3, ZrO_2, CdS and ZnS, have been used to promote photocatalytic oxidation of aqueous environmental pollutants [6]. But, among the different semiconductor materials, TiO_2 has been considered the most suitable photocatalyst due to some unique characteristics such as optical and electronic

* Corresponding author at: Department of Physics, University of Minho, Azurém Campus, 4800-058 Guimarães, Portugal.
E-mail address: salmon.landi@ifgoiano.edu.br (S. Landi).

http://dx.doi.org/10.1016/j.jphotochem.2017.05.047
1010-6030/

properties, chemical stability, availability, low-cost and their favourable redox properties for oxidation of pollutants [7].

However, TiO_2 has relatively low photo-quantum efficiency (that results from the fast recombination of photo-generated electron/hole pairs) and the large band gap energy in UV region (E_g, anatase phase ≅3.2 eV and rutile ≅3.0 eV, thus only making use of 3–5% of the solar spectrum that reach earth [8]) has limited the application of pure TiO_2 powder for industrial treatment of wastewater [9]. Several researches have tried to solve these problems through the use of dopants [10] and hybrid structures [11–13] to favour the degradation of different types of organic compounds. In particular, SiO_2-TiO_2 systems have received much attention due to their potential application in biomedical components, (as protective layer on NiTi surgical alloy [14]), antireflective coatings [15] or in photocatalytic systems [16]. According to Shifu and Gengyu [17], the addition of SiO_2 to TiO_2/bead showed better photocatalytic activity because it can raise the adsorbability of the photocatalyst. This circumstance restrains the temperature effects at which TiO_2 anatase phase transforms to rutile and prevents the agglomeration of TiO_2 particles. It is known, that the increase of the catalyst's surface area represents a strategy to obtain materials with higher photocatalytic efficiency, because only molecules that are in direct contact with the catalyst surface undergo photocatalytic degradation. Ang et al. [18] concluded that the SiO_2 in nitrogen-doped TiO_2-SiO_2 improves the thermal stability of the photocatalyst, decrease the TiO_2 particle size and enhances the formation of Brønsted acid sites. These sites are the hydroxyl groups placed on the surface of the catalyst that can trap the photogenerated holes and form $HO^{\bullet}$ radicals to carry out the oxidation processes.

Recently, photocatalysts using zeolites have also attracted great interest [19–25]. These microporous structures are currently used as catalysts, adsorbents and biomaterials [26–28]. Zeolites are crystalline aluminosilicate materials containing SiO_4 and AlO_4 tetrahedrons (elementary building units), which are linked at their corners through a shared oxygen atom, and this results in an inorganic macromolecule with a structurally different three-dimensional framework [29]. These microporous materials present higher surface area but most of them are internal formed by channels, channel intersections and/or cages and super-cages [30]. The high internal surface area of zeolites holds an excess of active sites that can both inhibit the aggregation of the semiconductor material as also bring the molecules of organic pollutants closer to the surface of the catalyst and still decrease the recombination of electron/hole pairs [31]. Furthermore, in the zeolite framework exists acid sites, responsible for the strong acidic catalytic behaviour of zeolites [30]. Particularly, HY zeolite belongs to the faujasite (FAU) structure characterized by the presence of super-cages with a diameter of 11.8 Å and an open diameter of 7.4 Å, high surface area and Brønsted and Lewis acid sites [26], which make it an important material for the preparation of composite materials.

This work reports the synthesis of SiO_2-TiO_2-HY composites in order to study the photocatalytic performance of cotton-textile substrates functionalized with these composites. It is unquestionable to admit that under the industrial point of view, the separation of photocatalytic powders from the liquid state and the subsequent recycling process are problematic due to the formation of aggregates. Another weakness in water treatment by using photocatalyst powders directly applied in the liquid is related to the penetration depth of solar light, which is limited because of strong absorption by both photocatalyst particles and dissolved organic contaminants. Immobilizing the photocatalyst on inert surfaces such as cotton material can surpass these problems. The option by textile materials is beneficial because, in general, they are very cheap, since they can be produced on a large industrial scale, present low weight and exhibit high mechanical flexibility, which is a very important feature since it allows its geometrical adaptability to the surfaces of water treatment tanks, which have already been installed in the industries. In addition, this strategy also opens the chance of photocatalyst recycling, decreasing the costs associated with the long settling times or filtration methods for its recovery. Therefore, many researches have addressed the cotton textile as alternative to immobilize the photocatalyst materials [32–34]. In our case, the photocatalytic ability of SiO_2-TiO_2 and SiO_2-TiO_2-HY coated textile substrates was evaluated by monitoring over time the degradation of Rhodamine B dye (RhB), a typical textile industry pollutant [35]. Moreover, the effect of calcination temperature of the composites on the photocatalytic activity was also studied. For this purpose, the as-prepared photocatalyst underwent a calcination process carried out at different temperatures, in particular 400, 500, 600 and 750 °C. The properties of the composites, prior the photocatalytic tests were obtained by Fourier transformed infrared (FTIR), X-ray diffraction (XRD), N_2 adsorption, UV–vis diffuse reflectance spectroscopy (DRS) and scanning electron microscopy (SEM).

2. Experimental, instruments and methods

2.1. Composites preparation

The sol-gel method was used to prepare silica-titanium sols, which were mixed with powder of ammonium Y zeolite ((NH_4)Y, Aldrich), according the procedure reported by Díaz et al. [36]. Tetraethyl orthosilicate (TEOS, Aldrich) and titanium tetra-isopropoxide (TTIP, SAFC) were employed as precursors for SiO_2 and TiO_2, respectively. Ethanol (Merck) and distillate water were used as solvents and ammonium hydroxide (NH_4OH, Aldrich) was utilized as a catalyst for hydrolysis. In a three-necked balloon was added TEOS in ethanol and ultra-pure water in the molar ratio of 1:3:49, respectively, under stirring at room temperature. In a separate flask, equal volumes of TTIP and ethanol (2.96 mL each one) were mixed and then added drop by drop during 1 h to the TEOS solution (TEOS:TTIP molar ratio of 1:4). After 30 min of stirring the pH was adjusted to 9.0 by using NH_4OH. To the resulting mixture was added the HY zeolite, previously calcined at 500 °C and kept in a desiccator, as to make 25% by weight of the sum TEOS, TTIP and HY. The mixture was refluxed at 70 °C for 6 h and the obtained gel was dried in an oven at 80 °C. The previous heat treatment of the zeolite was performed in order to convert (NH_4)Y in HY, since ammonium present was transformed in NH_3 and H^+. NH_3 desorbs and the presence of the H^+ increases the number of acid sites.

The composite particles were ground in a mortar and subjected to thermal treatment in a muffle furnace in a temperature range between 400 and 750 °C for 5 h with a heating rate of 6 °C/min. The different SiO_2-TiO_2-HY composites studied in this work, namely the ones no calcined, calcined at 400, 500, 600 and 750 °C were coded as STH, STH-400, STH-500, STH-600 and STH-750, respectively to facilitate the reading process. In addition, composites without HY zeolite were also produced, and these samples do not include "H" in their designation codes.

2.2. Composites characterization

Fourier Transform Infrared spectra were acquired on a Bomem MB104 spectrophotometer in the range between 4000 and 400 cm^{-1} by averaging 32 scans with a resolution of 4 cm^{-1} and an uncertain ±2 cm^{-1}. The composites were finely grinded with KBr and the powder mixture pressed in a mechanical press to form translucent pallet. The band between 570 and 600 cm^{-1} shows the most sensitive band in the HY zeolite structure and can be used to calculate framework Si/Al ratios according to the following

equation [30]:

$$x = 3.857 - 0.00621 w_{DR}, \quad (1)$$

where $x = (1 + \mathrm{Si/Al})^{-1}$ and w_{DR} is the wavenumber in the range 570–600 cm^{-1} related to zeolite specific double ring vibration.

Textural characterization of the materials was based on the analysis of N_2 adsorption isotherms, measured at −196 °C with a Nova 4200e (Quantachrome Instruments) equipment. Micropore volume (V_{micro}) and mesopore surface area (S_{meso}) were calculated by the t-method. Surface areas were calculated by applying the BET equation.

The powder XRD patterns (2θ = 5–65°) were recorded via a Bruker D8 Discover X-ray diffractometer using Cu Kα radiation (0.154056 nm) with a step of 0.02° and a time per step of 1 s. Before XRD measurements, the diffractometer was calibrated so that the nominal uncertain in the 2θ values is equal to ±0.004°. The profile peak shape, unit cell parameter of the HY zeolite (cubic symmetry), peak width of the TiO_2 and relative amount of each phase were extracted by the method of Rietveld using TOPAS-3 software. The framework Si/Al ratio in the composites with HY zeolite was determined by using the following equation [37]:

$$x = 5.348a - 12.898, \quad (2)$$

where x is defined above and a is the unit cell parameter (in nm) obtained from the curves adjusted by the Rietveld method. Since the simulation provided error in the fifth decimal place, an uncertainty of ±0.001 nm was assumed for all a values and the corresponding uncertainties of the Si/Al ratios were obtained through error propagation calculations. For comparison, these Si/Al ratios were also determined by using the Breck and Flanigen equation by utilizing the unit cell parameter values calculated for the (533), (642) and (555) reflections peaks of HY zeolite according to the ASTM D 3942-80 method [30,38]. However, the uncertainties of these Si/Al ratios were calculated by quadrature sum of the uncertainty arising from the error propagation calculation with the standard deviation of the mean for the three peaks mentioned above. Mean crystallite sizes of some catalysts of series ST were estimated from the (101) TiO_2 peak broadening using the Scherrer equation [39].

2.3. Functionalization of cotton fabrics

Firstly, the cotton fabrics (10 cm × 10 cm) were scoured with an aqueous solution (2.0 g/L) of a non-ionic and anionic detergent (kieralon OLB New) at 70 °C for 1 h to detach the impurities such as fat, powder, among others species. In this step, the fabric to solution weight ratio was equal to 10%. Subsequently, the samples were rinsed several times with distilled water to remove the detergent, and finally dried at room temperature. Afterwards, the cotton substrates were immersed over a period of 1 min in a composite/methanol suspension (1.00 g/L), previously homogenized by sonication, and then dried at room temperature [40]. This process was repeated three times in the same suspension, and finally the samples were cured at 100 °C for 10 min. It should be noted that the preparation of the composite/methanol suspension (used to enable the immersion of cotton substrate) was performed in such a way that, for each 1.0 g of cotton substrate, it was used 5.0 mg of the composite material.

2.4. Characterization of coated textiles

The band gap energy (E_g) represents an important characteristic of semiconductor materials since it determines their applications in photocatalytic processes. Thus, DRS as a simple and powerful spectroscopic tool was utilized to calculate E_g of the synthetized photocatalysts. This technique is similar to usual UV–vis spectroscopy where reflected light, instead of transmitted light, is collected. Analogous to transmittance for liquids, reflectance is a useful parameter to quantify the amount of light reflected by a solid sample. The diffused reflection measurements were acquired from a spectrophotometer ScanSpecUV-vis, ScanSci equipped with an integrating sphere assembly. Barium sulphate was used as a reference and the baseline was taken with the pristine cotton.

The E_g of the samples was calculated based on theory proposed by Kubelka and Munk according to the equation [13,41]:

$$F(R) = \frac{(1-R)^2}{2R} = \frac{K}{S}, \quad (3)$$

where $F(R)$ is the so called Kubelka–Munk function, R is the reflectance ($0 \le R \le 1$), K and S (that have units of inverse length) are the Kubelka-Munk absorption and scattering coefficients respectively [42]. The K is related to the incident photon energy (E) by means of the Tauc equation [43]:

$$(KE)^m = C_1(E - E_g), \quad (4)$$

where C_1 is a proportionality constant that depends on the properties of the material. The exponent m can take different values depending on the type of electron transition: for an indirect allowed transition $m = 1/2$ (such as anatase) and for a direct allowed transition $m = 2$ [41]. As $F(R)$ is proportional to K (according Eq. (3)) and considering an indirect allowed transition, Eq. (4) can be expressed as follows:

$$(F(R)E)^{0.5} = C_2(E - E_g). \quad (5)$$

In Eq. (5) $C_2 = (C_1 S^{-0.5})$ is a constant and $[F(R)E]^{0.5}$ is the well-known Kubelka–Munk transform. Therefore, by plotting $[F(R)E]^{0.5}$ versus E, it is possible to calculate the energy band gap E_g of the samples, which the extrapolation of the linear portion of this curve up to x-axis provided the E_g [44]. The E_g uncertainties were calculated by errors propagation from the linear fit parameters.

In order to characterize the morphology of the cotton textiles coated with the different photocatalysts materials, the cotton textiles were previously coated with a thin gold/palladium layer using a sputtering coating technique. Then, the analysis of samples morphologies were performed by SEM using a FEI Nova 200 FEG-SEM equipment operating at a maximum voltage of 15.0 kV. The distribution of the photocatalysts on the fibres was examined using SEM micrographs performed at a magnification of 5000×.

2.5. Photocatalytic activity and analytical procedure

A recirculation photocatalytic homemade reactor composes the experimental setup utilized to promote degradation of the RhB dye solution under simulated sunlight irradiation (Fig. 1). Initially, 0.4 L of RhB aqueous solution (5 mg/L) was circulated through the system for 4 h in the dark to reach adsorption-desorption equilibrium. After that time, the samples were irradiated for 2 h by using a 300 W lamp (Ultra-Vitalux E27, Osram), placed at a distance of about 25 cm above the cotton sample's surface, which simulated the solar irradiation. The UVA/B and visible light irradiance was around 1.0 and 0.5 $\mathrm{mW/cm^2}$, respectively. The absorbance of the RhB solution was monitored using a spectrophotometer (ScanSpecUV-Vis, ScanSci) in the 300–700 nm wavelength (λ) range. The photocatalytic degradation of RhB solution was followed by monitoring the solution absorbance maximum value (at λ_{max} = 553 nm) at time intervals of 1 h. The photocatalytic activity of the samples was evaluated taking into account the ratio of C/C_0 (calculated from the absorbance measurements), where C is the concentration of RhB after irradiation and C_0 is the concentration of the solution after has been forced to circulate

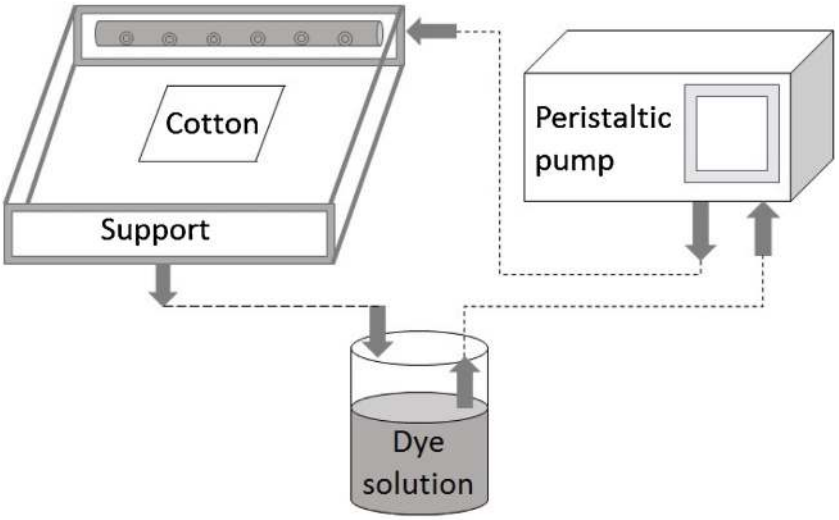

Fig. 1. Schematic diagram of the experimental setup, inspired from [45]. Placed at about 25 cm of the cotton surface, the lamp (not showed) and support are inserted in an opaque chamber.

in the system for 4 h in the dark; the instant just before of the irradiation was defined as zero time. In fact, C/C_0 was derived from the linear correlation verified between the concentration and the absorbance at λ_{max}, in the range of [RhB] = 0–20 mg/L, which implies that $C/C_0 = A/A_0$, where A (the absorbance after irradiation) and A_0 (the absorbance in the zero time) are measured by the spectrophotometer.

The analysis of total organic carbon (TOC) was performed in a L-TOC Total Organic Carbon Analyzer of Shimadzu coupled to ASI-L auto sampler of the same brand, by the NPOC method. TOC analysis is a quick and accurate alternative to the classical but lengthier biological oxygen demand (BOD) and chemical oxygen demand (COD) tests traditionally reserved for assessing the pollution potential of wastewaters.

The HPLC–MS set-up consisted of a Thermo Finnigan Lxq equipped with a UV–vis diode array detector in series with a mass detector and a C-18 reverse-phase column (2.6 μm, 100 mm × 2.1 mm i.d., Kinetex®). Acetic acid solution (0.1%, v/v) and acetonitrile were used as mobile phase at a flow rate of 0.4 mL/min. Positive and negative ionization modes were used. The quantitative analysis of the one reaction products (oxalic acid) was carried out by ion chromatography (DX-100, Dionex) using a conductivity detector, an ion exchange column AS11-HC and a guard column AG11-HC both from Dionex.

At last, the two functionalized textiles that presented better RhB degradation efficiencies were subjected to other photocatalytic degradation essays to evaluate its reusability. For that, they were washed in methanol/water mixture at 70 °C using an ultrasonic bath during 30 min before each run. All the experiments were performed in duplicate; differences in results from identical experiments were usually below 8%.

3. Results and discussion

3.1. Preparation and characterization of the samples

Fig. 2 shows the FTIR spectra of ST-600 and also for some composites compared with the zeolite HY spectrum. Typical bands of Si—O at 475 cm^{-1} [31] and around 555 cm^{-1} due to Ti—O [16] were identified in all SiO_2-TiO_2 composites, as exemplified by ST-600 spectrum in Fig. 2. This spectrum also exhibits a weak band at 936 cm^{-1} related to Si—O—Ti bonds, but this band was not detected in any SiO_2-TiO_2-HY composites, because probably it is overlapped by the intense bands of the zeolite structure. The strong bands assigned to the HY zeolite are present in all FTIR spectra of SiO_2-TiO_2-HY composites, namely: 461, 575, 723, 791, 1033, 1633 and 3433 cm^{-1} are identified in [46], except the first one that corresponds to bending modes of Si—O—Si linkage [47]. Only for the STH-750 composite, the bands at 791 and 723 cm^{-1} disappeared and new bands appeared at 784 and 671 cm^{-1}, which can be attributed to TiO_2 anatase phase [47] and Ti—O [17], respectively. On the other hand, the band that appears at 2924 cm^{-1} confirms the existence of —OH terminal [36], indicating the formation of acid groups during the gel formation, which eventually can be de-protonate [48] favouring the adsorption of RhB molecules or forming free radicals.

The framework Si/Al ratios obtained from Eq. (1) are listed in Table 1. The calcined composites showed different framework Si/Al ratios evidencing that the calcination treatment could affect the HY zeolite structure. The framework Si/Al ratio values for SiO_2-TiO_2-HY composites show that the preparation of the composites causes a slightly modification in the zeolite structure, since the calcination treatment origins an increase in the framework Si/Al ratios, suggesting a dealumination of the structure.

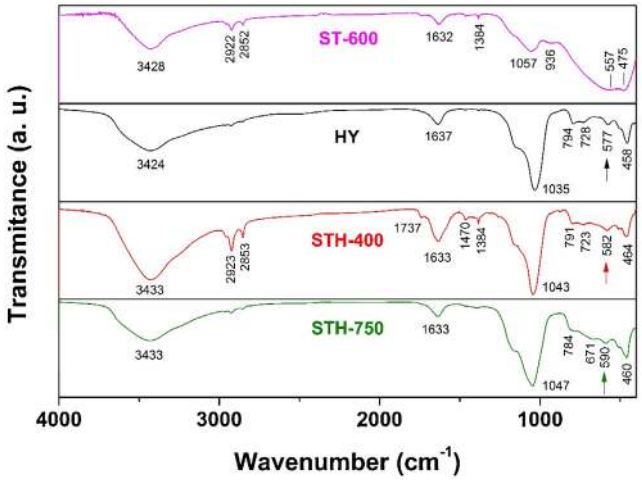

Fig. 2. FTIR spectrum of HY zeolite compared to the spectra of other composites. The arrows indicate the wavenumber used to calculate the Si/Al ratio by utilizing Eq. (1).

Table 1
Si/Al ratios of HY zeolite determined from FTIR and XRD data.

Sample	Framework Si/Al ratio		
	Double ring vibration (Eq. 1)	Rietveld analysis and Eq. (2)	ASTM D 3942-80 method and Breck and Flanigen equation
HY	2.7 ± 0.3	3.2 ± 0.1	3.4 ± 0.1
STH	2.5 ± 0.2	2.6 ± 0.1	2.7 ± 0.1
STH-400	3.1 ± 0.2	2.9 ± 0.1	2.7 ± 0.1
STH-500	3.0 ± 0.2	3.2 ± 0.1	3.1 ± 0.1
STH-600	3.3 ± 0.3	3.4 ± 0.1	3.3 ± 0.2
STH-750	3.9 ± 0.6	4.0 ± 0.1	4.4 ± 0.2

All composites were also analysed by XRD. In order to study the effect of the calcination temperature in the composites, Rietveld analysis was performed (Figs. S1 and S2 in Supplementary information). X-ray diffraction patterns of all prepared composites are shown in Fig. 3, except for those related to composites calcined at 600 °C. Identically to FTIR analysis, the XRD patterns also reveals the presence of the zeolite in the SiO_2-TiO_2-HY composites. All composites display the distinctive and similar peaks characteristic of the pattern of highly crystalline FAU zeolite structure [49].

Usually, anatase phase of TiO_2 shows better photocatalytic activity than that of the rutile and amorphous phase. For this reason, a calcination treatment was realized to obtain crystal phase TiO_2. However, factors such as surface area, crystal composition and material microstructures, also affect the catalytic performance of TiO_2 [50]. In the SiO_2-TiO_2 composites, the presence of SiO_2 inhibited the formation of rutile phase and the calcination treatment promotes the formation of nanosized TiO_2 anatase (insets Fig. 3).

The powder XRD pattern of the as-prepared composite (ST) that was not subjected to calcination showed amorphous phase (data not shown). Heating the same composite at 400 °C led to appearance of the most intense XRD peak (101) of the anatase (upper inset Fig. 3). This peak is broaden indicating a crystallite size of about 6.0 nm. Further rise of the temperature (500 °C) contributed to increased crystallinity, and other reflections of anatase such as (004), (200), (105), (211) and (204) have become visible (central inset Fig. 3). After calcination performed at 600 °C the catalyst showed no significant increase of the peak intensity and broadness (Fig. S1 in Supplementary information). Thus, the mean crystallite size obtained from the Scherrer equation is around 6.5 nm. Notable increase of the crystallinity was observed after calcination at 750 °C (lower inset Fig. 3). This was followed by increased average size (12 nm) of the crystallites and by well-defined anatase peaks.

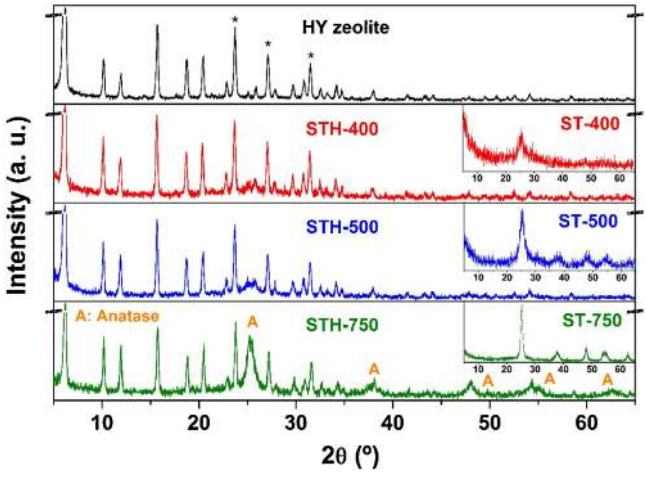

Fig. 3. X-ray diffraction patterns of HY zeolite and some prepared composites. Inset: X-ray diffraction patterns of ST composites calcined at 400, 500 and 750 °C, where the vertical and horizontal axis denotes the intensity (in arbitrary units) and angular peak position (2θ in degrees), respectively. The symbol (*) refers to peaks utilized to calculate the Si/Al ratios according to Section 2.2.

The Si/Al ratios of the zeolite framework calculated from the XRD diffractograms, according to the procedures described in Section 2.2, are listed in Table 1 showing a good consistency of these methods. The structural integrity of the zeolite was preserved even at high temperatures, which means that the preparation of the composites does not promote significant structural changes in the zeolite framework, in agreement with FTIR analysis.

It is know that the dehydration of zeolites results in increases of lattice parameters [38]. So, the decrease of the Si/Al ratio verified in the as prepared STH in comparison with HY zeolite can be explained by the hydration of the zeolite during the synthesis process. Obviously, the calcination process causes the inverse phenomena – dealumination, that suggests a decrease of the Brønsted acid sites.

The N_2 adsorption isotherms, measured at −196 °C, show that the calcination temperature affects the textural properties of the composites. The micropore volumes (V_{micro}) and mesoporous surface areas (S_{meso}) were calculated by the *t*-method, the BET surface areas (S_{BET}) by the BET equation and the total pore volume was obtained for $P/P_0 = 0.95$ (V_P). Table 2 displays the values obtained for the different samples.

As can be observed in Table 2, the presence of the HY zeolite enhances the surface area as well as the total pore volume of the SiO_2-TiO_2-HY composites, which is related to the high surface area of the HY zeolite. The increase of the calcination temperature modifies the textural properties of the composites, especially for those that do not contain the zeolite. It was observed a significant decrease in the surface area (S_{BET}) and pore volume (V_p) with the increase of the calcination temperature, where the decrease in the textural properties is more pronounced for the ST-600 composite.

The UV–vis diffuse spectroscopy was carried out in order to estimate the energy band gap of functionalized cotton substrates. The obtained band gap energies, regarding only the indirect allowed transition, are presented in Table 3. It is possible to observe that the presence of the HY zeolite in the composites did not affect the E_g values. Indeed, the band gap energies are higher than that

Table 2
Textural properties of the SiO_2, HY zeolite and some of the composites prepared.

Sample	S_{BET} (m^2/g)	S_{meso} (m^2/g)	V_{micro} (cm^3/g)	$V_{pP/Po=0.95}$ (cm^3/g)
SiO_2	28	30	0	0.053
HY	737	26	0.298	0.328
ST	492	30	0.249	0.295
ST-400	209	26	0.131	0.170
ST-600	108	108	0	0.100
STH	621	34	0.273	0.326
STH-400	527	31	0.243	0.292
STH-500	491	28	0.209	0.255

Table 3
E_g values for the functionalized cotton textiles.

Sample	E_g (eV)
ST/STH	3.58 ± 0.16/3.51 ± 0.11
ST-400/STH-400	3.43 ± 0.06/3.46 ± 0.13
ST-500/STH-500	3.41 ± 0.02/3.38 ± 0.06
ST-600/STH-600	3.41 ± 0.04/3.36 ± 0.10
ST-750/STH-750	3.38 ± 0.05/3.36 ± 0.18

ones observed for the TiO_2 anatase phase. This increment in the E_g values (in comparison with TiO_2) has also been reported by other authors in the SiO_2/TiO_2 systems [40,51], although the underlying mechanisms were still not fully explained.

Fig. 4 depicts the Kubelka–Munk transform (plotted against incident photon energy) and the corresponding diffuse reflectance spectra (inset) for the cotton textile samples coated with ST and STH-750 photocatalysts, which presented the largest and smallest E_g values.

It can be observed, that these photocatalysts exhibited very similar light diffuse reflections at wavelength longer than 350 nm, and therefore their band gap values are also similar.

SEM analysis provides information on the morphology and dispersion of the photocatalysts on the textile substrate surface. The SEM micrographs of pristine cotton and the cotton textiles coated with ST, ST-400 and STH-400 photocatalysts are shown in Fig. 5.

SEM analysis shows that in general, for all the samples, the photocatalysts are irregular in shape, randomly organized and tends to form agglomerates. By a further observation of the samples morphology, it is possible to notice that the different photocatalysts do not exhibit the same degree of dispersion and coating along the cotton fibres. Actually, the coating appears to be much more effective for the ST and ST-400 photocatalysts than for the STH-400 composite photocatalyst. It can be observed that for the case of STH-400 photocatalyst, the cotton surface fibres are much less coated by this composite and therefore possess at its surface less photocatalyst material, which could be available to be activated by incident light.

This behaviour suggests that the anchoring process of the composite photocatalyst (SiO_2-TiO_2 photocatalyst mixed with the zeolite HY) is less effective than for the ST and ST-400 photocatalysts. Under this assumption, the STH-400 composite may have become entrapped in the void spaces between the cotton fibres as a result of the loss of surface adhesion. Under this context, photocatalytic efficiency should tend to decrease since some of the particles/agglomerates of the composite photocatalyst may become shaded (covered) by superficial cotton fibres and therefore may not be so available to be activated by light in order to participate in the degradation reactions of the organic pollutants and thus, leading to lower photodegradation ability.

3.2. Photocatalytic results

The photocatalytic activity was tested by studying the bleaching of RhB ($C_{28}H_{31}ClN_2O_3$) aqueous solution as a function of time. In the following discussion, all cotton textile samples were functionalized in suspensions prepared with the same concentration of 1 g/L, according to Section 2.3. Initial tests showed that by using suspensions with concentrations ranging between 0.5 and 2 g/L there are no significant variations in the photocatalytic degradability of RhB dye (Fig. S3 in Supplementary information). So, it was decided to select the suspension with a concentration of 1 g/L to compare the photocatalytic efficiencies of all functionalized cotton textiles. For aqueous solutions of low concentrations, the Beer–Lambert law determines that a solution's concentration of a particular compound is proportional to its absorbance. The decrease of RhB content was estimated by measuring at different irradiation times, the peak intensity (occurring at a wavelength around 553 nm) of its optical absorption spectrum. Fig. 5 shows the decrease in the concentration of RhB aqueous solution (that is, decrease of its C/C_0 ratio), both under dark conditions (over 4 h, that is negative time) as with light irradiation (throughout 2 h, that is positive time), while it was circulating onto the cotton substrates.

Analysing Fig. 6, it is possible to observe that, in general, the textile samples with better adsorption characteristics also showed the highest photocatalytic degradation ability. Also, the composites without zeolite (Fig. 6a) showed higher adsorption capacities compared with those containing the HY zeolite (Fig. 6b) at the same calcination temperature. These results suggest that part of the microporous volume of the zeolite can be inaccessible for the RhB molecules (as will be shown later, its smallest dimension is equal to 11.94 Å), since the pore apertures of HY are about 7.4 Å. In addition, for calcination temperatures above 500 °C, all the samples showed lower adsorption capacities. This behaviour could be due to the calcination process carried out at gradual higher temperatures, which enables the crystalline growth and generating a composite with smaller surface area as it is confirmed by the N_2 adsorption results (see Table 2).

In particular, Fig. 6a depicts the variation on the C/C_0 ratio of bare RhB dye solution (i.e. without the textile substrates) and of RhB dye solution in the presence of pristine cotton. RhB degradation of 5% and 8%, over a period of 2 h, were achieved for bare RhB solution and pristine cotton, respectively, which can be attributed to photolysis. Meanwhile, the cotton samples coated with SiO_2 and HY zeolite could decompose RhB over a period of time equal 2 h, achieving an efficiency of 33% (calculated from data in Fig. 6a) and 38% (calculated from data presented in Fig. 6b), respectively. These materials are not photocatalytic, but they present Brønsted acid sites that can be de-protonated at a wide range of pH making the surface negatively charged. This effect increases the adsorption of RhB on the surface of these materials favouring the photolysis and even contributing for degradation of RhB molecules from the released of H^+ ions. According to the obtained results, it can be seen that the high calcination temperatures (i.e. 600 and 750 °C) are detrimental to photocatalytic performance. However, for the lower calcination temperature,

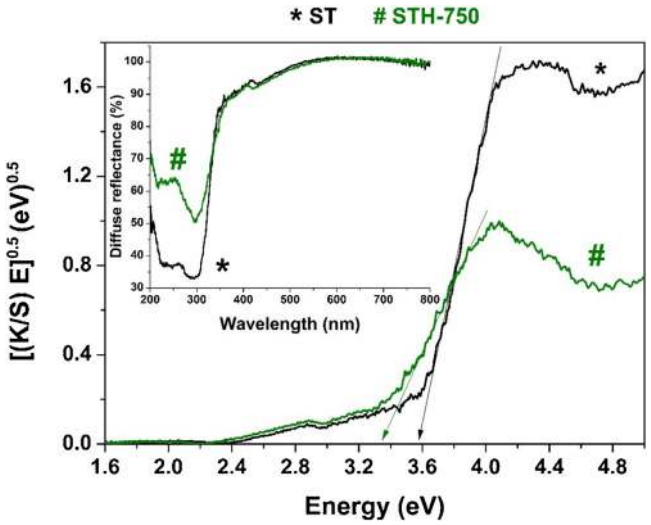

Fig. 4. Plot of Kubelka–Munk transform against incident photon energy for cotton textiles coated with ST and STH-750 photocatalysts. Inset shows the DRS corresponding.

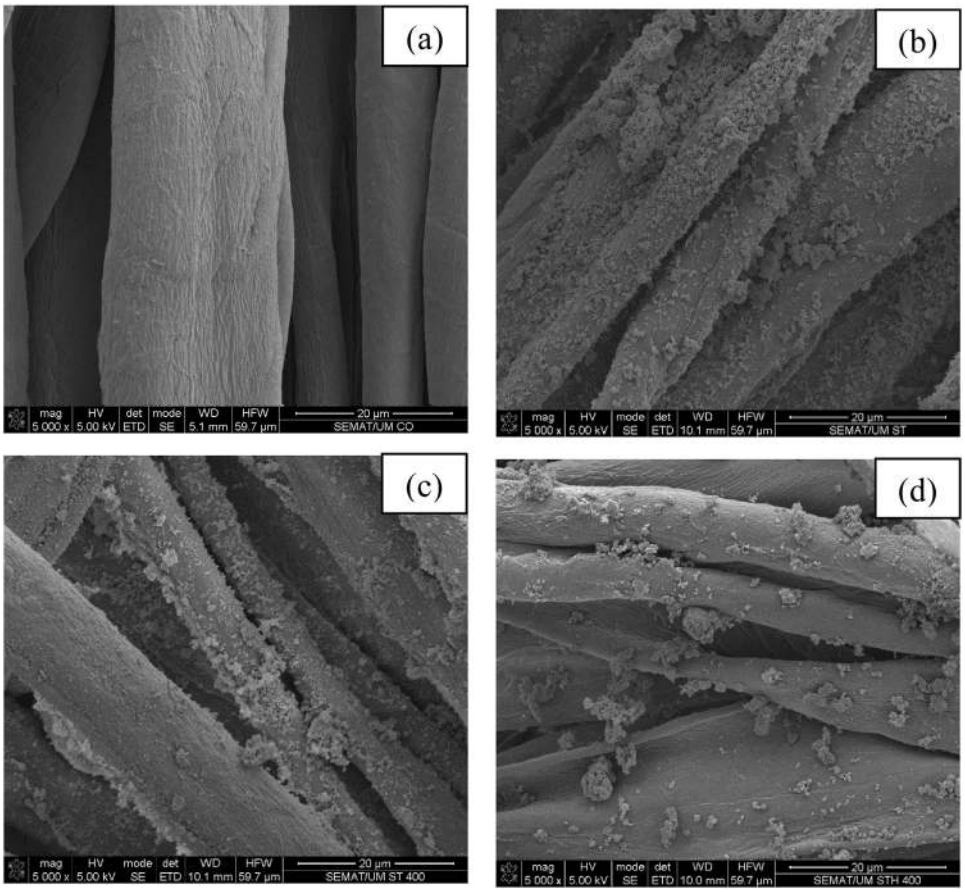

Fig. 5. SEM micrographs of cotton pristine cotton (a) and cotton textiles coated with (b) ST, (c) ST-400 and (d) STH-400 photocatalysts at a magnification of 5000×.

400 °C, the photocatalytic performance of the composites undergoes a moderate increase. Additionally, a comparison between Fig. 6a and b shows that the presence of the HY zeolite in the composites did not favour their photocatalytic properties for RhB dye degradation during 2 h under sunlight irradiation. It was verified (data not showed) that the concentration of the STH-400 suspensions, used for functionalization of the cotton textile, need to be increased much more (from 1 to 5 g/L) to achieve a similar photocatalytic performance to the once reached by ST-400 sample functionalized with the suspension at 1 g/L.

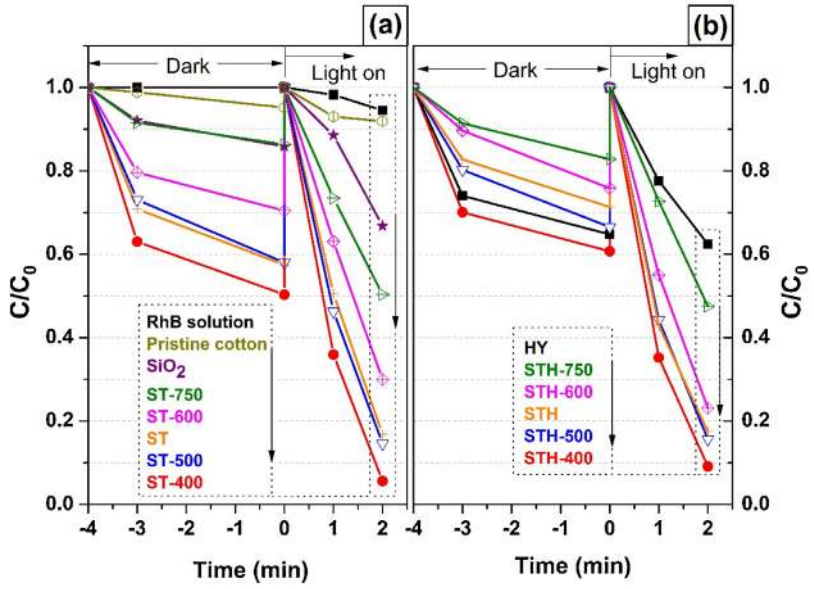

Fig. 6. Decrease of RhB solution concentration in the dark ($-4\,h \leq time \leq 0$) and photodegradation of RhB solution ($0 \leq time \leq 2\,h$) under similar sunlight irradiation.

The decrease of photocatalytic characteristics of coated textile substrates, after having been subjected to four consecutive experiments was estimated (Fig. S4 in Supplementary information). Results showed that the photocatalytic decomposition of RhB reached around 94% (ST-400 sample) and 86% (STH-400 sample) after the first run. However, after the fourth run (with the same samples), these values were about 78% for ST-400 sample and 66% for sample STH-400. This may be related to the removal of some composite particles from the surface of the textile substrates during the washing process.

The time variation of the UV–vis spectra for ST-400 coated cotton substrate is showed in Fig. 7. It can be observed that besides the bleaching of the RhB solution, related to the RhB dye degradation, the absorption spectrum also exhibited slight hypsochromic shifts suggesting that the cleavage of the RhB structure is dominant in relation to loss of the ethyl groups (N-de-ethylation process) [33]. This behaviour was verified for all samples. However, it is observed that the absorption peak intensities of RhB aqueous solutions, in contact with the textile substrates coated with ST-750 and STH-750 composites, for example, still maintain relatively high values and thus, evidencing weak degradation of the RhB dye (Fig. S5 in Supplementary information). In particular, the UV–vis spectrum after 2 h of irradiation (Fig. 7) suggests a small amount of fully de-ethylated RhB molecules considering that the wavelength of the major absorption peak intensity is around 498 nm [52]. It may also be probable that some RhB molecules remain on the cotton fabrics after the photocatalytic treatments (Fig. S6 in Supplementary information).

Fig. 8 shows the results obtained for TOC measurements and RhB degradation, from the UV–vis spectra, after 2 h of the photocatalytic assays. These results refer to aqueous solutions that have been treated with textile substrates coated with STH-400 and ST-400 composites. Although these RhB aqueous solutions showed a slightly difference in its discoloration after 2 h under sunlike irradiation, the remaining TOC was substantially different, since it corresponds to about 57% (STH-400) and 11% (ST-400) of its initial content. These dissimilar performances in terms of mineralization suggest that a part of the photocatalyst (SiO_2-TiO_2) may be formed within the zeolite cavities and thus, making it unavailable to participate in the RhB dye adsorption/degradation process [53]. On the other hand, different C/C_0 ratios obtained from the UV–vis and TOC measurements confirms the presence of

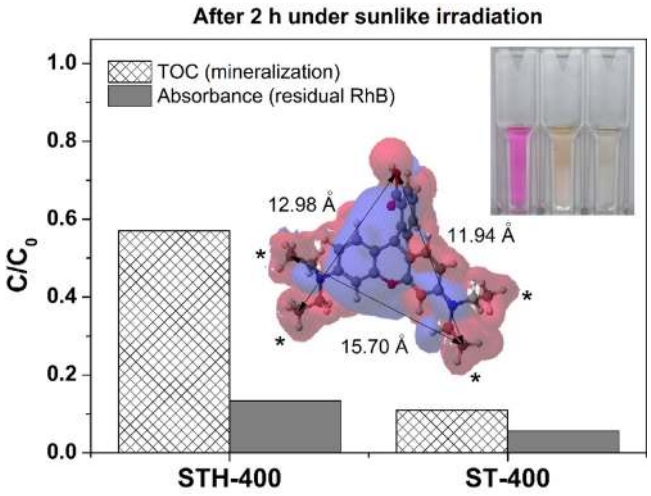

Fig. 8. TOC and RhB solution dimensionless concentrations after 2 h of similar solar irradiation for RhB solutions treated with cotton substrates coated by STH-400 and ST-400 composites. The corner inset shows the original RhB solution (left) and final appearance of the solutions treated with STH-400 (center) and ST-400 (right) samples. The molecular dimension of RhB molecule is given in the same figure where the red and blue areas correspond respectively to the positive and negative surface charges. The symbol (*) refers to the ethyl groups in the RhB molecule. (For interpretation of the references to color in this figure legend, the reader is referred to the web version of this article.)

intermediate products due to the incomplete degradation of the RhB molecules.

The products of RhB degradation were analysed and identified by using high performance liquid chromatography coupled to electrospray ionization mass spectrometry (HPLC-ESI–MS) and ion chromatography (IC) techniques. The chromatograms (total ion current, TIC) ESI-positive mode showed ion peaks differed by 28 amu in sequence, which is in agreement with the sequential loss of the ethyl groups from the RhB molecule, which appears at 18.5 min (Fig. 9). Although, the bottom chromatogram shows a broad peak centred at 19 min, the extracted chromatograms for m/z 443 show that the amount of RhB is lower for the treatment with ST-400 than that observed for STH-400 samples (Inset Fig. 9). The de-ethylation intermediate with $m/z = 331$ (loss of 4 ethyl groups by RhB) was identified at 10.05 min confirming the UV–vis results. In addition, C—C bond cleavages other than de-ethylation were

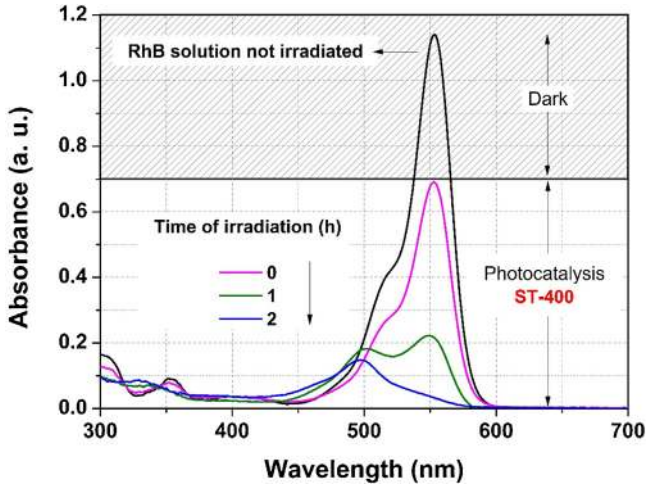

Fig. 7. Time variation of UV–vis spectrum of RhB aqueous solution under similar sunlight irradiation and in the presence of ST-400 coated cotton textile substrates.

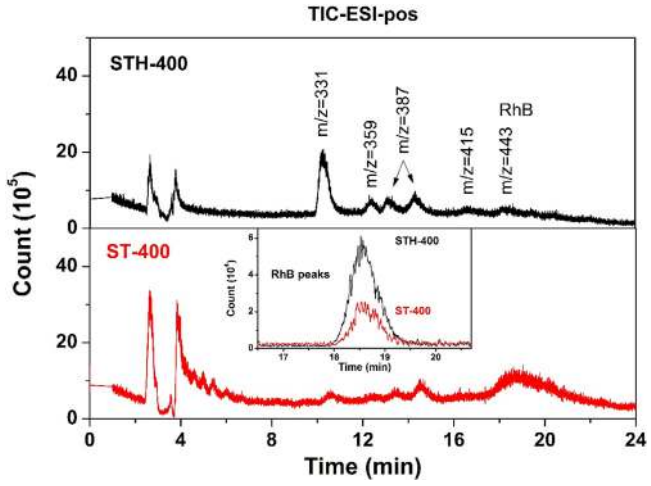

Fig. 9. TIC chromatograms (ESI-pos) of the RhB solution after 2 h of similar solar irradiation in the presence of samples coated with STH-400 (top) and ST-400 (bottom) composites. Inset: extracted peaks of the RhB ion.

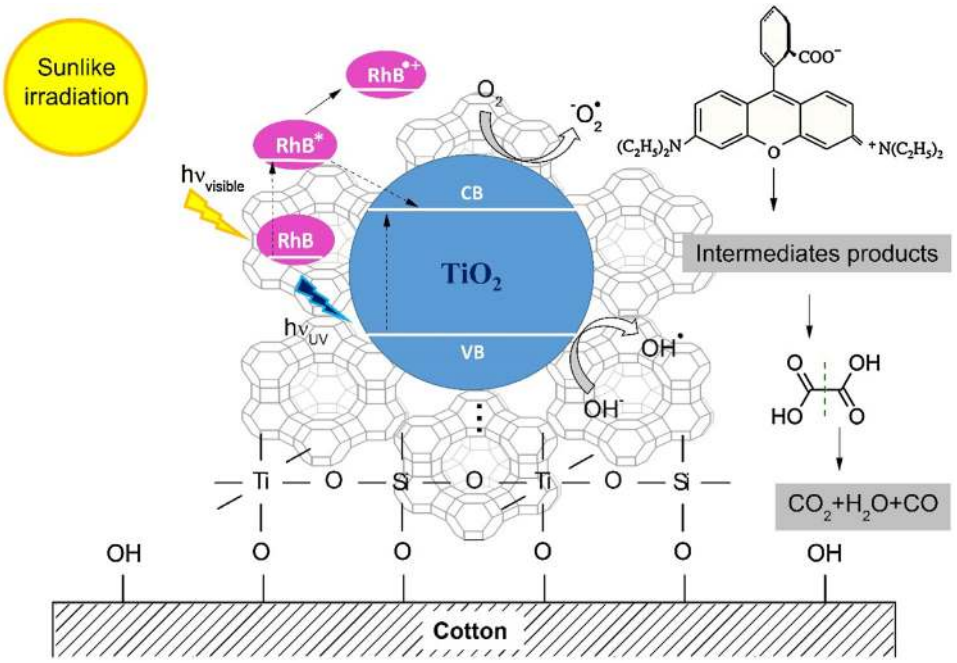

Fig. 10. Schematic anchoring of composites on cotton textile and photocatalytic mechanism of RhB degradation for the ST composites (without background) and the STH composites (with background).

confirmed in the negative ESI mode by the presence of ions with mass 97, 155, 179 and 195 [54]. Furthermore, the concentration of oxalic acid analysed by ion chromatography (data not shown), present in the final solutions treated with ST-400 and STH-400 samples was 0.18 and 0.49 ppm, respectively. These results prove that the RhB also suffered a degradation with higher extent.

3.3. Proposed mechanisms

Based in our photocatalytic results, we proposed a probable mechanism for the anchorage of the composites on the cotton textiles and for the RhB degradation (Fig. 10). As it is known, the cotton fibers possess several surface hydroxyl groups, which are capable to form stable bonds with the composites during the cure process [16]. In the proposed photocatalytic mechanism the role of ultraviolet (UV) and visible light is highlighted (Fig. 10). In the presence of light the electron transfer from excited RhB molecules by to conduction band (CB) of the TiO_2 occurs principally at excitation wavelengths in the visible region (around 553 nm), according to the absorbance spectrum of RhB molecule (Fig. 7). On the other hand, according to Table 3, the wavelengths related to the band gap energies, considering the uncertainties, vary between 332 and 390 nm, therefore, in the UV region of electromagnetic spectrum. Finally, numerous intermediate products obtained in the solutions treated with the ST-400 and STH-400 composites suggests the formation of different oxygen radicals due to reactions between the charge carriers and the dissolved species in solution [35]. The scheme that appears as a background in Fig. 10 represents the zeolite structure that possess interconnecting channels and cavities typical of a microporous material. Fig. 10 also shows the presence of SiO_2 that besides acting as a binder, can helps to increase the available surface area of the photocatalyst [34].

In applications for traditional industrial sectors (e.g. petroleum refining and in the petrochemical and fine chemical industries), the microporous structure of zeolite (providing large surface areas and acidity) are beneficial since it enables the transfer of chemical reagents between intra-crystalline spaces, and therefore bringing them more easily into contact, thereby promoting the occurrence of chemical reactions and improving its kinetic [55].

On the other hand, several scientific works demonstrated that good photocatalyst should possess a high specific surface area available for the adsorption and decomposition of the organic pollutants [56]. This is the idea that initially guided our work. In order to achieve this goal, it was anticipated that the addition to the SiO_2-TiO_2 photocatalyst of a support with high surface area and acidity, as is the case of zeolite structures, could fulfil this purpose. This expectation was due to some important characteristics that determine the role played by zeolites as catalysts such as (1) acting as a support to provide better dispersion of SiO_2-TiO_2, (2) providing sites that can prevent charge recombination processes and (3) delivering acid sites that can degrade the formed intermediates.

The work herein developed concerns a photocatalytic process that, by definition, not only requires the presence of light but also requires that the semiconductor material should be able to absorb light in an effective way. In this sense, despite the existence of some important characteristics of zeolite materials, which determine the role they play as catalysts, other phenomena may have been responsible for the slightly decrease of the photocatalytic properties for the composite photocatalyst series (initially we anticipated an improvement of its photocatalytic ability). In an attempt to explain what may have happened, we suggested that part of composite photocatalyst (STH series) experienced a loss of surface adhesion (as can be inferred by the analysis of SEM micrographs) and might have fallen into the spaces (holes) between the fibres so getting shaded/covered by some of them. As a result, its photocatalytic efficiency tends to decrease because there should be less composite photocatalyst available to be activated by light in order to participate in the redox reactions of the organic pollutants.

4. Conclusions

Photocatalytic materials have been produced by functionalization with SiO_2-TiO_2 and SiO_2-TiO_2-HY composites on cotton textiles. The differences observed in the photocatalytic activity

are related to the structural and textural properties, since the band gap energy was not affected by the calcination treatment. FTIR and XRD results showed that the main effect on the HY zeolite in the composites has been the dealumination of the framework. The dealumination observed in the composites with the increase of framework Si/Al ratios can be related to the decrease in the acidity of the zeolite. Therefore, the loss of acid sites explains the lower photocatalytic efficiency of composites subjected to high calcination temperature. In this work, it has been found that the calcination temperature of 400 °C favoured the formation of anatase phase while causing no major textural changes in the properties of the composites. The observed changes in UV–vis spectra, the TOC measurements and the chromatography results suggest that under similar solar irradiation and in the presence of the ST-400 sample, the RhB molecules not only lost N-ethyl groups but also suffered a high degradation process. On the other hand, it was observed that ST and STH photocatalyst series, at the same calcination temperature, on the cotton textiles presented similar decolourization capacities, although the STH series needed the use of a smaller amount of TiO_2-SiO_2 photocatalyst due to the HY properties previously mentioned. As a final remark, the results suggest that under the studied conditions, ST photocatalyst series are more favorable to deposit on cotton fibres than the STH composite photocatalyst series.

Acknowledgements

The authors thank CAPES from Brazil for the financial support of this work. This work is also a result of project "AIProcMat@N2020 – Advanced Industrial Processes and Materials for a Sustainable Northern Region of Portugal 2020", with the reference NORTE-01-0145-FEDER-000006 and the project BioTecNorte (operation NORTE-01-0145-FEDER-000004), supported by Norte Portugal Regional Operational Programme (NORTE 2020), under the Portugal 2020 Partnership Agreement, through the European Regional Development Fund (ERDF). This work also has been funded by ERDF through COMPETE2020 – Programa Operacional Competitividade e Internacionalização (POCI), Project POCI-01-0145-FEDER-006984 – Associate Laboratory LSRE-LCM and by national funds through FCT – Fundacão para a Ciência e a Tecnologia for project PTDC/AAGTEC/5269/2014 and Centre of Chemistry (UID/QUI/00686/2013 and UID/QUI/0686/2016).

Appendix A. Supplementary data

Supplementary data associated with this article can be found, in the online version, at doi; 10.1016/j.jphotochem.2017.05.047.

References

[1] C. O'Neill, F.R. Hawkes, D.L. Hawkes, N.D. Lourenço, H.M. Pinheiro, W. Delée, J. Chem. Technol. Biotechnol. 74 (1999) 1009–1018.
[2] D. Suteu, C. Zaharia, A. Muresan, R. Muresan, A. Popescu, Environ. Eng. Manag. J. 8 (2009) 1097–1102.
[3] D. Shahidi, R. Roy, A. Azzouz, Appl. Catal. B: Environ. 174 (2015) 277–292.
[4] S. Malato, J. Blanco, A. Vidal, D. Alarcón, M.I. Maldonado, J. Cáceres, W. Gernjak, Sol. Energy 75 (2003) 329–336.
[5] A.R. Khataee, M.N. Pons, O. Zahraa, J. Hazard. Mater. 168 (2009) 451–457.
[6] M.R. Hoffmann, S.T. Martin, W. Choi, D.W. Bahnemannt, Chem. Rev. 95 (1995) 69–96.
[7] A. Fujishima, T. Rao, D. Tryk, J. Photochem. Photobiol. C: Photochem. Rev. 1 (2000) 1–21.
[8] C. Chen, W. Ma, J. Zhao, Chem. Soc. Rev. 39 (2010) 4206–4219.
[9] H. Zabihi-Mobarakeh, A. Nezamzadeh-Ejhieh, J. Ind. Eng. Chem. 26 (2015) 315–321.
[10] A. Di Paola, E. Garcıa-López, S. Ikeda, G. Marcı, B. Ohtani, L. Palmisano, Catal. Today 75 (2002) 87–93.
[11] Y. Wang, X. Yang, Z. Wang, X. Lv, H. Jia, J. Kong, M. Yu, J. Photochem. Photobiol. A: Chem. 325 (2016) 55–61.
[12] J. Zhang, X. Zhang, S. Dong, X. Zhou, S. Dong, J. Photochem. Photobiol. A: Chem. 325 (2016) 104–110.
[13] A. Farhadi, M.R. Mohammadi, M. Ghorbani, J. Photochem. Photobiol. A: Chem. 338 (2017) 171–177.
[14] S. Cao, T. Liu, Y. Tsang, C. Chen, Appl. Surf. Sci. 382 (2016) 225–238.
[15] X. Li, J. He, ACS Appl. Mater. Interfaces 5 (2013) 5282–5290.
[16] E. Pakdel, W.A. Daoud, J. Colloid Interface Sci. 401 (2013) 1–7.
[17] C. Shifu, C. Gengyu, Surf. Coat. Technol. 200 (2006) 3637–3643.
[18] T.P. Ang, C.S. Toh, Y.F. Han, J. Phys. Chem. C 113 (2009) 10560–10567.
[19] S. Azimi, A. Nezamzadeh-Ejhieh, J. Mol. Catal. A: Chem. 408 (2015) 152–160.
[20] M.R. Eskandarian, M. Fazli, M.H. Rasoulifard, H. Choi, Appl. Catal. B: Environ. 183 (2016) 407–416.
[21] K. Guesh, C. Márquez-Álvarez, Y. Chebude, I. Díaz, Appl. Surf. Sci. 378 (2016) 473–478.
[22] K. Guesh, Á. Mayoral, C. Márquez-Álvarez, Y. Chebude, I. Díaz, Microporous Mesoporous Mater. 225 (2016) 88–97.
[23] M. Khatamian, S. Hashemian, A. Yavari, M. Saket, Mater. Sci. Eng. B 177 (2012) 1623–1627.
[24] P. Mohammadyari, A. Nezamzadeh-ejhieh, RSC Adv. 5 (2015) 75300–75310.
[25] R. Nagarjuna, S. Roy, R. Ganesan, Microporous Mesoporous Mater. 211 (2015) 1–8.
[26] A. Corma, H. Garcia, Eur. J. Inorg. Chem. 2004 (2004) 1143–1164.
[27] L. Ferreira, J.F. Guedes, C. Almeida-Aguiar, A.M. Fonseca, I.C. Neves, Colloids Surf. B: Biointerfaces 142 (2016) 141–147.
[28] C.M.A.S. Freitas, Soares O.S.G.P, J.J.M. Órfão, A.M. Fonseca, M.F.R. Pereira, I.C. Neves, Green Chem. 17 (2015) 4247–4254.
[29] J. Weitkamp, Solid State Ionics 131 (2000) 175–188.
[30] A.C. Lopes, M.P. Silva, R. Gonçalves, M.F.R. Pereira, G. Botelho, M. Fonseca, S. Lanceros-mendez, I.C. Neves, J. Phys. Chem. C 114 (2010) 14446–14452.
[31] J. Esmaili-Hafshejani, A. Nezamzadeh-Ejhieh, J. Hazard. Mater. 316 (2016) 194–203.
[32] A. Bozzi, T. Yuranova, I. Guasaquillo, D. Laub, J. Kiwi, J. Photochem. Photobiol. A: Chem. 174 (2005) 156–164.
[33] D. Wu, H. Wang, C. Li, J. Xia, X. Song, W. Huang, Surf. Coat. Technol. 258 (2014) 672–676.
[34] T. Yuranova, R. Mosteo, J. Bandara, D. Laub, J. Kiwi, J. Mol. Catal. A: Chem. 244 (2006) 160–167.
[35] H. Jia, W. He, W.G. Wamer, X. Han, B. Zhang, S. Zhang, Z. Zheng, Y. Xiang, J.-J. Yin, J. Phys. Chem. C 118 (2014) 21447–21456.
[36] R. Díaz, S. Macías, E. Cázares, J. Sol-Gel Sci. Technol. 35 (2005) 13–20.
[37] W. Lutz, C.H. Ruscher, D. Heidemann, Microporous Mesoporous Mater. 55 (2002) 193–202.
[38] J. Kaduk, J. Faber, Rigaku J. 12 (1995) 14–34.
[39] J.O. Carneiro, S. Azevedo, F. Fernandes, E. Freitas, M. Pereira, C.J. Tavares, S. Lanceros-Méndez, V. Teixeira, J. Mater. Sci. 49 (2014) 7476–7488.
[40] B. Xu, J. Ding, L. Feng, Y. Ding, F. Ge, Z. Cai, Surf. Coat. Technol. 262 (2015) 70–76.
[41] J.O. Carneiro, S. Azevedo, F. Fernandes, E. Freitas, M. Pereira, C.J. Tavares, S. Lanceros-Méndez, V. Teixeira, J. Mater. Sci. 49 (2014) 7476–7488.
[42] V. Džimbeg-malčić, Ž. Barbarić-mikočević, K. Itrić, Tech. Gaz. 18 (2011) 117–124.
[43] J. Tauc, R. GRIGOROVICI, A. VANC, Phys. Status Solidi 15 (1966) 627–637.
[44] M.F. Abdel Messih, M.A. Ahmed, A. Soltan, S.S. Anis, J. Photochem. Photobiol. A: Chem. 335 (2017) 40–51.
[45] F. Harrelkas, A. Paulo, M.M. Alves, L. El Khadir, O. Zahraa, M.N. Pons, F.P. van der Zee, Chemosphere 72 (2008) 1816–1822.
[46] I. Kuz'niarska-Biernacka, P. Parpot, C. Oliveira, A.R. Silva, M.J. Alves, A.M. Fonseca, I.C. Neves, J. Phys. Chem. C 118 (2014) 19042–19050.
[47] S.M. Kemdeo, V.S. Sapkal, G.N. Chaudhari, J. Mol. Catal. A: Chem. 323 (2010) 70–77.
[48] T. Kuzniatsova, Y. Kim, K. Shqau, P.K. Dutta, H. Verweij, Microporous Mesoporous Mater. 103 (2007) 102–107.
[49] M.M.J. Treacy, J.B. Higgins, Collect. Simulated XRD Powder Patterns Zeolites Fifth Revis. Ed. (2007).
[50] Y. Li, T. Sasaki, Y. Shimizu, N. Koshizaki, J. Am. Chem. Soc. 130 (2008) 14755–14762.
[51] M.V. Roldan, Y. Castro, N. Pellegri, A. Duran, J. Sol-Gel Sci. Technol. 76 (2015) 180–194.
[52] J. Zhao, T. Wu, K. Wu, K. Oikawa, H. Hidaka, N. Serpone, J. Phys. Chem. B 102 (1998) 5845–5851.
[53] M. Klimenkov, S.A. Nepijko, W. Matz, X. Bao, J. Cryst. Growth 231 (2001) 577–588.
[54] K. Yu, S. Yang, H. He, C. Sun, C. Gu, Y. Ju, J. Phys. Chem. A 113 (2009) 10024–10032.
[55] C. Martínez, A. Corma, Coord. Chem. Rev. 255 (2011) 1558–1580.
[56] M. Bellardita, M. Addamo, A. Di Paola, G. Marcì, L. Palmisano, L. Cassar, M. Borsa, J. Hazard. Mater. 174 (2010) 707–713.